Macromolecules
ARTICLE

Macromolecules **2009**, *42*, 7889–7896 **7889**
DOI: 10.1021/ma901294t

Onset Kinetics of Thermal Degradation of Ultrathin Polyacrylamide Films

S. Mukherjee,[†] Mojammel H. Mondal,[†] M. Mukherjee,*[,†] B. P. Doyle,[‡,⊥] and S. Nannarone[‡,§]

[†]*Surface Physics Division, Saha Institute of Nuclear Physics, 1/AF, Bidhannagar, Kolkata-64, India,* [‡]*Laboratorio Nazionale TASC, INFM-CNR, S.S. 14, km 163.5, Area Science Park, 34012 Basovizza (TS), Italy, and* [§]*Dipartimento di Ingegneria dei Materiali e dell'Ambiente, Università di Modena e Reggio Emilia, Via Vignolese 905, 41100 Modena, Italy*

Received June 16, 2009; Revised Manuscript Received August 17, 2009

ABSTRACT: There are several pathways through which a polymer can degrade such as thermal, photoinduced, biological, chemical and mechanical. The thermal degradation process of polymers is widely studied because of both academic and industrial interest. Here we have investigated the kinetics of thermal degradation and structural modification of polyacrylamide ultrathin films as a result of heat treatment at the degradation onset temperature. The chemical analysis of the material was performed using X-ray photoelectron spectroscopy (XPS) and near-edge X-ray absorption fine structure (NEXAFS) spectroscopy. The formation of imide functionalities was found to occur on the polymer chains with simultaneous breakdown of amide groups. The kinetics of the degradation products obtained from quantitative analysis of the XPS spectra shows that the thermal degradation of the major part of the polymer occurs within the first 30 min of heating at the onset temperature of 220 °C. The rate of degradation was found to saturate after ~3 h of heating. The structural aspects of the heated films were studied using X-ray reflectivity (XRR). Analysis of the reflectivity data shows that the thickness of the film decreases and the electron density increases after prolonged heating at 220 °C. From the amplitude of the reflectivity data, it was found that the interfacial morphology of the film stays almost unmodified and the film retains the polymeric property even after undergoing thermal degradation. The final onset degradation product obtained was ultrathin films of polymer containing 60% and 40% mono- and bicyclic imide functionalities, respectively.

1. Introduction

Polymers are an extraordinarily versatile class of materials and are all around us in everyday use, in rubber, in plastics, in resins and in adhesives and adhesive tapes.[1] The common structural feature in polymer is the presence of long covalently bonded chains of atoms. Polymers such as aromatic polyimides and polycarbosiloxanes are widely used in microelectronic, aviation, liquid crystal displays, and optoelectronic and separation industries because of their excellent thermal stability, good chemical resistance, mechanical strength and low dielectric constants.[2−5] Recently a growing interest has developed in water-soluble polymers for their versatility and various application potentials in physical and biological systems.[6−14] Commercial water-soluble polymers such as polyacrylamide (PAM), polyethylene oxide (PEO), poly(acrylic acid) (PAA), polyvinyl pyrrolidone (PVP), etc. are extensively employed in cosmetics and in pharmaceuticals.[15]

However, low thermal stability of many polymeric materials prevents their wider commercial application.[16,17] The reduction in mechanical properties with time at elevated temperatures is a key limiting factor in the use of polymers in engineering application. This reduction in properties is attributed to the degradation of the polymer caused by breaking and modification of chemical bonds in the polymer chains. Degradation reactions are generally irreversible and alter the physical and chemical properties of the polymer. There are several pathways through which a polymer can degrade, viz., thermal, photoinduced, biological, chemical and mechanical.[18] The thermal degradation process of polymers is widely studied because of both academic and industrial interest.[18−22] It is influenced by a variety of factors including mode of synthesis, molecular weight, presence of additives or impurities, presence or absence of oxygen, etc. It is observed that some factors stabilize while other factors accelerate degradation depending on the type of polymer and the mechanism of thermal degradation.[20] Studies of polymer degradation are also of interest for environmental reasons as they can sometimes produce toxic byproducts.

The polymer PAM which finds its use in a wide range of industrial applications such as commercial water treatment and oil recovery is generally nontoxic.[18] However, the monomer (acrylamide) is known to be neurotoxic and there are concerns over the possibility of PAM degrading back to the monomer. Few studies on the thermal degradation of polyacrylamide have been conducted in the past.[18−20] In thermogravimetric studies by Van Dyke and Kasperski,[19] where PAM in powder form was heated at 10 °C/min from 30 to 600 °C, it was suggested that there are certain temperature regions where thermal degradation primarily occurs. It was shown by the authors that the degradation mechanism starts at 220 °C. It is well-known that dynamical studies may yield different products as compared to isothermal studies, therefore it becomes extremely important to know the details of degradation mechanisms at the onset of degradation. Information thus obtained may act as a crucial input for the development of polymer materials for high temperature applications. Although ultrathin water-soluble polymer films have recently become the subject of extensive research,[8−14] thermal degradation studies on such systems are absent in the literature. We have performed a study of the kinetics of thermal degradation as a function of time of ultrathin polyacrylamide films at the onset temperature of degradation. In this paper, we report

*Corresponding author. E-mail: manabendra.mukherjee@saha.ac.in.
[⊥]Present address: Department of Physics, University of Johannesburg, PO Box 524, Auckland Park 2006, South Africa.

Published on Web 09/08/2009

chemical and structural modifications due to annealing of polyacrylamide thin films at the onset temperature of degradation under vacuum conditions. The kinetics of thermal degradation of the films has been studied using NEXAFS, XPS, and XRR.

We used NEXAFS spectroscopy to examine the chemical bonds for the identification of samples. The technique involves the excitation of core electrons from inner shells into unoccupied molecular orbitals by tunable photons across the absorption edges of selected atomic core levels and also through detailed fitting of the spectral line shape. This technique is useful to detect the presence of specific bonds in molecules which in turn can be assigned to particular chemical moieties and functional groups. Moreover the absorption line shape contains detailed information on the local structure around the absorbing atom. In XPS the photons are absorbed by atoms in the sample leading to ionization and emission of a core electron. The shape of each peak and the binding energy depends on the chemical state of the emitting atoms. Therefore this technique provides information about the chemical bonding of the atom in question. As the number of emitted photoelectrons is directly proportional to the number of emitting atoms the peak area of a particular spectrum provides quantitative information about an elemental species. Here XPS was used for identification and quantification of degradation products and determination of the kinetics of the change of their concentration. It may be noted here that XPS and NEXAFS have been used as complementary techniques and the final results obtained were the outcome of an iterative process where the results from one technique were used as a feedback for the other and the cycle repeated several times. X-ray reflectivity is one of the most powerful techniques to study the structural aspects of thin homogeneous systems. This nondestructive method allows one to measure the thickness of a film and its electron density as a function of depth in terms of the refractive indices of homogeneous layers. The structural parameters of the films were determined from the analysis of the XRR data. In the present study we observe that formation of imide functionalities occurs on the polymer chains with simultaneous breakdown of amide groups. The long chain polymeric nature of the thin film samples was unaltered after long time annealing. The kinetics of the degradation products obtained from quantitative analysis shows that the thermal degradation of the major part of the polymer occurs within the first 30 min of heating at the onset temperature of 220 °C. The rate of degradation is observed to decrease with duration of thermal treatment and the concentrations of the degradation products saturate after 3 h of annealing. The final products of degradation are found to be imide functionalities on the polymer chains with monocyclic imide being the major constituent.

2. Experimental Details

Sample Preparation. A powder of high molecular weight (M_w = (5−6) × 10^6) polyacrylamide (Polysciences, USA) was taken as the starting material for the experiment. A solution of concentration 4 mg/mL was prepared from the powder source. Ultrathin films from the solution were prepared on silicon substrate by spin coating at a spinning speed of 4000 rpm. During the spinning, clean and warm (60 °C) air was gently flowed over the sol using a homemade arrangement to facilitate faster evaporation of water. The thicknesses of the films were ∼300 Å. Before coating, the silicon wafers were cleaned by the RCA cleaning method, where the wafers were boiled at 100 °C for about 15 min in a solution of H_2O, NH_4OH, and H_2O_2 (volume ratio, 2:1:1). The wafers were then rinsed with Millipore water. Apart from cleaning, this treatment enhances the hydrophilicity of the silicon surface by introducing −OH dangling bonds on the surface which helps better attachment of water-soluble polymers to the substrate.

Near-Edge X-ray Absorption Fine Structure (NEXAFS). From the NEXAFS studies the bonds and the functional groups present in the samples were identified.[23] The as-coated samples were prepared by drying PAM films at 105 °C for 3 h under vacuum conditions. Different dried films were heated in vacuum at 220 °C outside the experimental chamber for different durations. In all cases the heating rate was kept at 5 °C/min. The absorption studies were performed in an ultrahigh vacuum (UHV) chamber[24] installed at the bending magnet beamline BL-8.1 L BEAR[25] of the ELETTRA synchrotron at Trieste, Italy. The ring was operated in the multibunch mode at 2 GeV with a current between 100 and 250 mA. The beam intensity $\Phi(\hbar\omega)$ was monitored by measuring the drain current $I_{mesh}(\hbar\omega)$ from a passivated gold mesh inserted in the beam between refocusing optics and experimental chamber. The relative energy calibration was performed by comparing the absorption features of the gold mesh. Absolute energy calibration of the monochromator was carried out using the absorption lines of Ne and N_2 gases. The NEXAFS spectra at the C, N, and O K-absorption edges were acquired in the total electron yield (TEY) mode by, measuring the drain current $I_{sample}(\hbar\omega)$. The sample was biased at −20 V with respect to ground in order to overcome sample charging problems and to maximize the signal-to-noise ratio. The X-ray absorption data were collected with X-ray incidence at 45° with the electric field vector $\vec{E}$ parallel to the sample surface. Several consecutive scans were registered on each spot in order to estimate the effect of beam damage. In order to take into account of the energy dependence of the incident photon flux, the $I_{sample}(\hbar\omega)$ was normalized to the drain current from a clean gold sample $I_{Au}(\hbar\omega)$, featuring an unstructured absorption cross section[26,27] in the energy range of interest as follows

$$A(\hbar\omega) = \frac{I_{sample}(\hbar\omega, t)}{I_{mesh}(\hbar\omega, t)} \times \frac{I_{mesh}(\hbar\omega, t')}{I_{Au}(\hbar\omega, t')}$$

where t and t' represent the two different times when the sample and the clean gold were measured respectively. The drain current, $I_j(\hbar\omega)$, from sample, mesh or Au reference may be written as $I_j(\hbar\omega) = V_j(\hbar\omega)C_j(\hbar\omega)\alpha_j(\hbar\omega)\Phi(\hbar\omega)|_{j=sample,mesh,Au}$ where $V(\hbar\omega)$ is the sampled volume, $C(\hbar\omega)$ is the electron-per-photon conversion function and $\alpha(\hbar\omega)$ is the optical absorption coefficient. From the above equations one obtains

$$A(\hbar\omega) = F(\hbar\omega)\frac{\alpha_{sample}(\hbar\omega)}{N_{Au}\sigma_{Au}(\hbar\omega)} \quad (1)$$

where

$$F(\hbar\omega) = \frac{V_{sample}(\hbar\omega)C_{sample}(\hbar\omega)}{V_{Au}(\hbar\omega)C_{Au}(\hbar\omega)}$$

can be calculated from eq 1 with the help of the approximation that far from absorption edge $\alpha_{sample}(\hbar\omega)$ can be represented as $\sum_k N_k\sigma_k(\hbar\omega)$, where N_k is the atomic density and $\sigma_k(\hbar\omega)$ the atomic absorption cross section (can be found tabulated[26,27]) for chemical species k. With the help of known $F(\hbar\omega)$ and assuming it to be constant over a particular scan range one can represent, to a first approximation, the NEXAFS data in terms of the optical absorption coefficient of an unknown sample. For the purpose of data analysis a linear background $L(\hbar\omega)$ was subtracted from $\alpha_{sample}(\hbar\omega)$ which approximates to the removal of the atomic contribution in the spectral range. Therefore the NEXAFS data given here, $\Delta\alpha(\hbar\omega) = \alpha(\hbar\omega) - L(\hbar\omega)$, actually represents the molecular contribution to the optical absorption coefficient over the atomic background.

X-ray Photoelectron Spectroscopy (XPS). Elemental quantification and chemical characterization of the samples were obtained by XPS analysis using an Omicron Multiprobe (Omicron NanoTechnology, UK) spectrometer fitted with an

EA125 (Omicron) hemispherical analyzer. The system base pressure was 5×10^{-10} mBar. The sample was mounted on a stainless steel (SS) sample plate and held in position by two thin SS strips placed on two opposite sides of the sample. The ends of the strips were spot-welded to the sample plate. A monochromated Al Kα X-ray source with X-ray photon energy of 1486.7 eV operated at 150 W and having spot-size ~1 mm was utilized for the experiments. The analyzer pass energy was kept fixed at 20 eV for all the scans. In order to remove surface water and water bound to the polymer matrix the sample was dried under UHV conditions for 3 h at 105 °C before the XPS measurements. The annealing was performed using resistive heating with a heater attached to the base of the sample stage. The heating rate was kept at 5 °C/min and was controlled by changing the voltage and current output of the heater power supply. The thermal degradation studies at the onset degradation temperature were performed by annealing a PAM film at the onset temperature 220 °C for different durations. First, the film was heated isothermally for 15 min at 220 °C. Thereafter the sample was allowed to cool down to room temperature and XPS measurements were conducted. The cycle described above was repeated for different time intervals amounting to a total isothermal annealing time of 8 h at 220 °C. During every heating cycle, residual gas analysis (RGA) scans were taken at regular time intervals in order to identify any gas released from the sample during the degradation process. At the end of each annealing cycle the sample was allowed to cool down to room temperature and XPS measurements were conducted thereafter.

X-ray Reflectivity. X-ray reflectivity is one of the best nondestructive methods to measure thickness and electron density of polymeric films. We have used this technique here to study the structural aspects of the dry polyacrylamide films. X-ray reflectivity data were collected in our laboratory setup with Cu Kα radiation obtained from a copper sealed tube anode (2.2 kW, Bruker AXS, D8 Discover). Specular scans with identical incoming and outgoing angles for X-rays were taken as a function of momentum transfer vector q normal to the surface ($q = (4\pi/\lambda) \sin \theta$, with θ equal to the incident and the reflected angles of the X-ray and $\lambda = 1.54$ Å, the wavelength of the radiation).

3. Results and Discussion

Near Edge X-ray Absorption Fine Structure (NEXAFS) Spectroscopy. In the present work 280 eV, 394 and 522 eV were chosen for the calculation of the $\alpha_{sample}(\hbar\omega)$ using eq 1 at C, N, and O K-edges respectively. The $F(\hbar\omega)$ evaluated for the PAM sample using the tabulated cross section values was utilized to calculate the optical absorption coefficients for the heat treated samples at the above-mentioned energies. In order to perform the spectroscopic fingerprinting of the material the spectra were deconvoluted using a series of Gauss−Lorentz sum functions, asymmetric Gaussian peaks and an error function step multiplied by an exponential decay term.[23] The peaks below the step have been fitted using symmetric Gauss−Lorentz peaks whereas the σ^* resonances in the continuum were fitted using asymmetric Gaussian functions. The latter were constructed by modifying a Gaussian function so that the peak width depends linearly on photon energy instead of being a constant.[23] The results obtained from the fits are summarized in Table 1.

C K-Edge. The carbon K-edge NEXAFS spectra at different stages of annealing of the films are shown in Figure 1a. The π^* region is dominated by a sharp maximum at around 288 eV. From the raw spectra it can be easily observed that with longer heat treatment this peak appears to decrease in intensity and become wider and asymmetric toward the higher photon energy side along with a shift of its center of gravity toward lower photon energies. The fitted C K-edge spectrum for the sample annealed for 8 h is shown in Figure 2a. The results obtained from fitting of the spectra provided in Table 1A show that notable changes in the peak positions and areas are observed for the films heated for ≥ 2 h at 220 °C. In the case of the as-coated sample the dominating peak in the π^* region of the spectrum occurs at 288.1 eV and is attributed to a π^* resonance in the C═O bond present in the amide functional group (−N−C═O)[28−30] of PAM. In the case of the sample annealed for 2 h, this peak was found to split into two components centered at 286.8 and 287.9 eV. For the sample heated for 8 h the C═O peak was found to split into three components centered at 287.0, 287.7, and 288.3 eV. The collective area under the C═O π^* peaks was observed to decrease considerably for the sample heated for 2 h as compared to that for the as-coated film. However, after 2 h of thermal treatment the total area values for the C═O π^* peak tends to saturate as observed from comparison of the same for the samples heated for 2 and 8 h at 220 °C. Apart from this dominating π^* peak the C K-edge spectra comprises another narrow feature at around 284.7 eV. The intensity of this peak was found to increase with progressive thermal treatment. It may be noted that in the N−C═O group the N−C bond may possess a partial π-character due to a conjugation with the adjacent C═O bond.[28,31−33] The lowest energy peak in the C K-edge spectra can therefore be speculatively correlated to C═N π^* resonances.[34] The increase in area under this peak with duration of heat treatment suggests a possible formation of degradation products having N−C═O and/or C═N bonds in their structure. The region of σ^* resonances for all the four samples exhibits a similar feature consisting of a relatively narrow peak in the range 289−290 eV due to C−H σ^* transitions,[23,33−35] the area under which increases with progressive thermal treatment, and two broad features observed in the range 294−296 eV and 301−303 eV which can readily be attributed to C−C/C−N and C═O/C═N σ^* resonances[33−36] respectively. The areas under these two peaks are found to remain almost unchanged with the duration of annealing. The above observations therefore suggest reduction of amide functionality in the annealed film and formation of two additional compounds having N−C═O groups in their structure with the major part of the modifications occurring within the first 2 h of thermal treatment.

N K-edge. The nitrogen K-edge NEXAFS spectra at different stages of annealing of the films are shown in Figure 1b. In assigning the features present in the nitrogen K-edge spectra we have been guided by the assignments in the carbon K-edge. The fitted N K-edge spectrum for the sample annealed for 8 h is shown in Figure 2b. The results obtained from fitting of the spectra, as shown in Table 1B, show the advent of two peaks at 399.3 and 400.1 eV in case of the sample annealed for 30 min at the onset degradation temperature (220 °C). The former was observed to vanish with progressive heating and may be attributed to formation of some intermediate degradation product whereas the latter may be assigned to the presence of aliphatic imine (C═N)[29] species in the annealed samples. From the nitrogen spectra it can also be clearly observed that the sharp π^*-like peak at 401.3 decreases in intensity with the duration of thermal treatment. This peak has been attributed to the N−H σ^* transition.[29,30,33] The decrease in intensity of this peak indicates the breakdown of amide groups of PAM with subsequent formation of products having different functionalities. The intensity of the peak occurring at 402.4 eV was found to increase with annealing time. Since the C−N bond in the functional group N−C═O is known to have a partial π-character due to a conjugation with the adjacent carbonyl bond as mentioned earlier, this feature therefore has been

Table 1. Peak Positions and Their Speculative Assignments for (A) Carbon, (B) Nitrogen, and (C) Oxygen K Edge Resonances As Obtained from Fitting of NEXAFS Spectra

A. C K-edge

sample	normalized area (%)	position (eV)	fwhm (eV)	assignment
as-coated	3.68	284.7	1.29	C=N π*
	39.17	288.1	0.70	C=O π*
	13.88	289.6	1.94	C–H σ*
	22.89	295.3	6.36	C–C/C–N σ*
	20.38	301.5	6.36	C=O/C=N σ*
220 °C, 30 min	3.01	284.5	1.42	C=N π*
	39.18	288.1	0.74	C=O π*
	14.63	289.5	2.15	C–H σ*
	23.02	294.8	6.74	C–C/C–N σ*
	20.16	301.4	6.82	C=O/C=N σ*
220 °C, 2 h	5.41	284.8	1.33	C=N π*
	3.70	286.8	0.89	C=O π*
	26.33	287.9	1.07	C=O π*
	23.02	289.3	2.69	C–H σ*
	23.55	295.7	6.52	C–C/C–N σ*
	17.99	302.3	6.41	C=O/C=N σ*
220 °C, 8 h	6.94	284.7	1.37	C=N π*
	9.04	287.0	1.64	C=O π*
	12.73	287.7	0.73	C=O π*
	6.46	288.3	0.97	C=O π*
	25.07	289.3	2.70	C–H σ*
	23.44	296.1	6.30	C–C/C–N σ*
	16.30	302.7	6.29	C=O/C=N σ*

B. N K-edge

sample	normalized area (%)	position (eV)	fwhm (eV)	assignment
as-coated	23.18	401.3	1.06	N–H σ*
	3.22	402.4	0.77	N–C=O π*
	25.02	405.3	4.10	C–N σ*
	48.58	412.2	7.38	C=N σ*
220 °C, 30 min	4.93	399.3	1.43	intermediate product
	2.94	400.1	0.63	C=N π*
	17.58	401.3	1.22	N–H σ*
	3.87	402.5	0.84	N–C=O π*
	31.18	406.1	5.57	C–N σ*
	39.47	412.7	7.39	C=N σ*
220 °C, 2 h	8.39	400.0	1.23	C=N π*
	11.21	401.3	0.96	N–H σ*
	10.00	402.4	1.05	N–C=O π*
	23.93	407.0	4.45	C–N σ*
	46.46	413.7	8.15	C=N σ*
220 °C, 8 h	12.46	400.0	1.16	C=N π*
	5.43	401.3	0.85	N–H σ*
	10.75	402.4	1.24	N–C=O π*
	29.64	407.4	4.61	C–N σ*
	41.71	414.5	7.91	C=N σ*

C. O K-edge

sample	normalized area (%)	position (eV)	fwhm (eV)	assignment
as-coated	30.91	530.2	1.11	C=O π*
	10.06	533.2	2.00	C=O σ*/Si–O σ*
	29.72	538.1	5.52	C=O σ*/Si–O σ*
	29.32	543.4	7.81	C=O σ*/Si–O σ*
220 °C, 30 min	27.56	530.0	1.42	C=O π*
	8.02	533.1	1.93	C=O σ*/Si–O σ*
	34.88	537.4	5.42	C=O σ*/Si–O σ*
	29.54	542.4	7.35	C=O σ*/Si–O σ*
220 °C, 2 h	21.94	529.7	1.26	C=O π*
	10.27	530.4	1.94	C=O π*
	7.83	533.1	2.05	C=O σ*/Si–O σ*
	30.91	537.9	5.09	C=O σ*/Si–O σ*
	23.19	543.1	6.27	C=O σ*/Si–O σ*
220 °C, 8 h	23.10	529.5	1.24	C=O π*
	10.52	530.4	1.93	C=O π*
	9.63	533.0	2.22	C=O σ*/Si–O σ*
	32.05	537.9	4.77	C=O σ*/Si–O σ*
	24.71	543.1	6.18	C=O σ*/Si–O σ*

assigned to transitions of N1s electrons to π^* (CO) orbitals[33] and can be correlated to the C=N π^* transition observed at around 284.7 eV in the C K-edge spectra. The intense σ^* peaks in the regions 405−408 and 412−415 eV have been

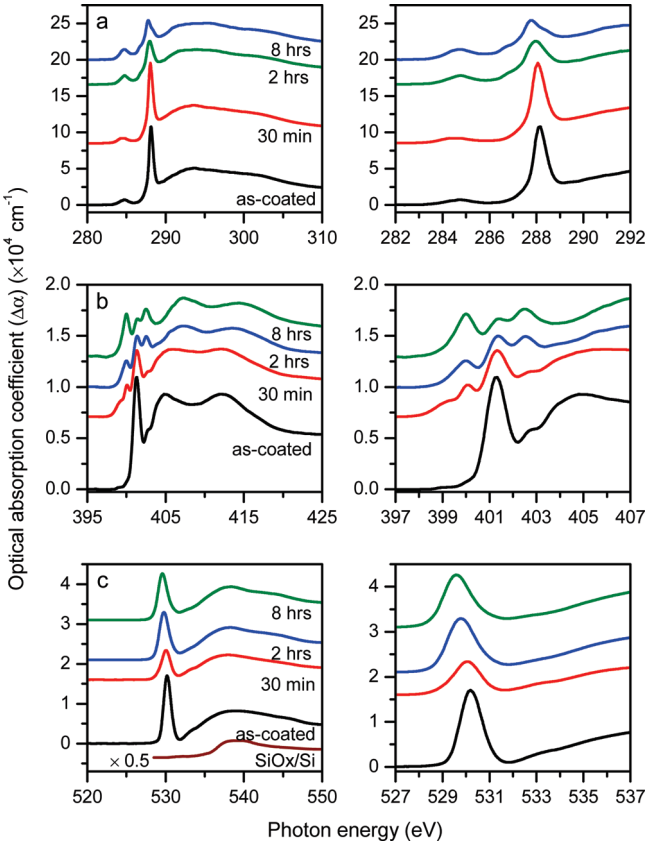

Figure 1. Left panel: Sequence of (a) C K-edge; (b) N K-edge, and (c) O K-edge normalized NEXAFS spectra of PAM heated at the onset temperature (220 °C) for different duration. Right panel: Expanded view of the low energy region of the left panel.

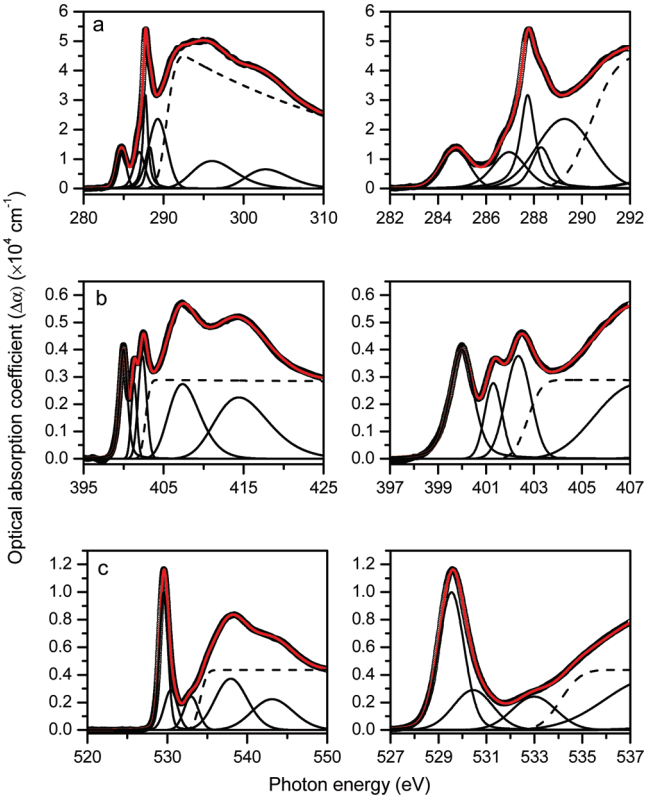

Figure 2. Left panel: Representative curve fits of (a) C K-edge; (b) N K-edge, and (c) O K-edge NEXAFS spectra for the PAM film annealed for 8 h at the onset temperature (220 °C). Right panel: Expanded view of the low energy region of the left panel.

attributed to C−N and C=N σ^* transitions respectively. These peaks were observed to shift toward higher energies with their intensities remaining almost unaltered with heating duration.

O K-Edge. The O K-edge NEXAFS spectra of the untreated and annealed PAM samples are shown in Figure 1c. The spectra can be observed to be dominated by a strong π^* resonance at ~530 eV which is due to transfer of O1s electrons to the C=O π^* orbitals.[23] The fitted O K-edge spectrum for the sample annealed for 8 h is shown in Figure 2c. The results obtained from fitting of the spectra, as shown in Table 1C, illustrate that after 2 h of annealing at the onset degradation temperature (220 °C) the single π^* peak at around 530 eV disappears along with the advent of two peaks at around 529.5 and 530.4 eV. These observations indicate the breakdown of amide groups with simultaneous formation of products with at least two different functionalities having C=O bonds in their structure. The above observations are in excellent agreement with those obtained from the C K-edge spectra where reduction of the amide functionality along with formation of two additional compounds having N−C=O groups on annealing were observed. It may be noted here that the native oxide present on the substrate surface also contributes to the σ^* region of the oxygen absorption spectra from the polymer films. The O K-edge absorption spectrum from a clean substrate with native oxide is shown in Figure 1c. As the contribution from the native oxide corresponds to the region containing broad humps in the polymer spectra, the peaks occurring in this region were therefore not considered for analysis.

Taken together, the NEXAFS studies indicate that, on prolonged annealing of thin films at the degradation onset temperature, the breakdown of the amide group of the polymer occurs due to possible imidization[3,4] of the polymer resulting in formation of mono- and bicyclic imide groups on the polymer chains. Similar observations have also been reported by Van Dyke et al.[19] in their thermogravimetric studies on the degradation of PAM in the temperature range 220−340 °C. The possible degradation products are shown in Figure 3. We note that although NEXAFS spectra enable spectroscopic fingerprinting of the functional groups, elemental quantification cannot be performed because of the sensitivity of this technique toward unsaturated bonds.[28,30] Therefore XPS data are required for quantification purposes.

X-ray Photoelectron Spectroscopy (XPS). For this quantitative chemical analysis we have performed XPS core level studies of a PAM sample at different stages of thermal treatment. In Figure 4, the variation of carbon, nitrogen, and oxygen atomic concentrations are shown. The carbon concentration is found to be almost constant throughout the duration of the thermal treatment whereas the concentrations of nitrogen and oxygen exhibit an initial drop. This has been attributed to a possible release of NH_3 and H_2O gases from the sample as part of the thermal degradation process.[19] However, the above gases were not detected in the RGA scans performed during our XPS experiments which may be due to the fact that the amount of the gas was below the detection limit of the instrument. Changes in shape of the photoelectron spectra were also observed as a function of duration of thermal treatment. In order to curve fit the XPS spectra the guideline from the results obtained from the NEXAFS studies were used. The spectra were curve fitted

(a) Structure of PAM:

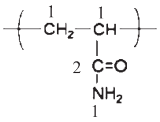

(b) Structure of monocyclic imide compound:

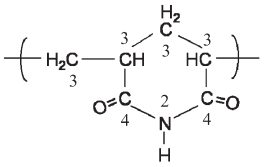

(c) Structure of bicyclic imide compound:

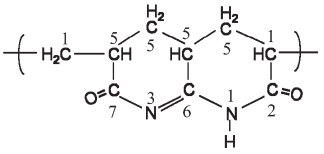

Figure 3. (a) Structure of PAM; the proposed byproducts of thermal degradation due to annealing the ultrathin films at the degradation onset temperature: (b) monocyclic and (c) bicyclic imide functional groups on a chain as obtained from NEXAFS studies. The different carbon and nitrogen environments in PAM monomer units and monocyclic, bicyclic imide groups are indicated.

after subtraction of a linear background arising due to the secondary electrons. It may be noted here that the C1s spectrum from the pure polymer contains two well-separated peaks corresponding to the different carbon environments as indicated in Figure 3. It can also be clearly observed that the unit −CH2CHCONH− which is the same monomer repeat unit for the pure polymer as well as in the product having bicyclic imide structures in its chains. A sum of two Gauss−Lorentz (G−L) peaks corresponding to sites 1 and 2 having area ratio 2:1 with a peak separation of ∼3.1 eV[37] was used to represent the photoelectron peak from pure PAM and the above unit present in the bicyclic imide functionality. Henceforth in this manuscript we shall refer to this unit as the "amide-bicyclo imide combined" unit and the corresponding peak as the "combined" peak for convenience. The carbon atoms of the monocyclic imide structure corresponding to the two different chemical environments 3 and 4 were represented by a sum of two G−L peaks having area ratio 2:1 and peak separation ∼3.2 eV.[37] Similarly the carbon atoms corresponding to the sites 5, 6, and 7 in the bicyclic imide structure were represented by a sum of three G−L peaks having area ratio 4:1:1 and peak separations ∼1.5 and ∼3.4 eV[30] with respect to the major peak position. Henceforth in this manuscript the former and latter groups of peaks shall be referred to as the "monocyclic" and "bicyclic" peaks in the C1s spectra respectively for convenience. In order to minimize the number of fit parameters the combined and monocyclic peaks were merged and fitted as a single set of two peaks due to identical functional forms and peak positions. The nitrogen spectra consist of contributions from the three different nitrogen chemical environments as shown in Figure 3. Three G−L peaks corresponding to the three different nitrogen sites were used for the fitting of the N1s spectra. The O1s XPS data were fitted with two G−L peaks related to the carbonyl (C═O) groups present in the functionalities of the constituents and the silicon oxide peak from the SiO_2/Si substrate. In Figure 5, the fitted C1s, N1s, and O1s core level XPS spectra at three different stages of thermal treatment are shown. The combined, monocyclic,

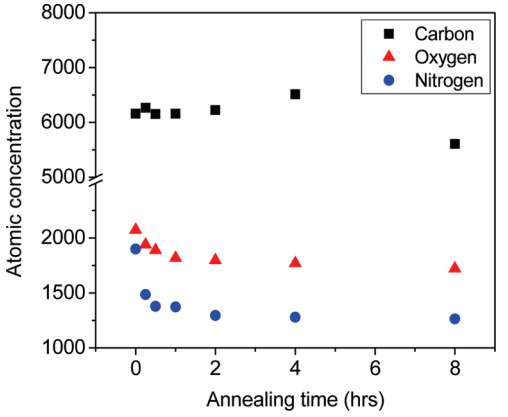

Figure 4. Variation of carbon, nitrogen, and oxygen atomic concentrations in the PAM sample with annealing time as obtained from XPS studies.

and bicyclic peaks are indicated in the spectra for carbon and nitrogen. The carbonyl peak and the oxide contribution from the substrate are indicated in the oxygen spectra.

In order to obtain the individual concentrations of pure polymer and mono- and bicyclic imide functional groups, the following constraints were imposed while curve fitting the core level XPS spectra:

(i) Concentration of monocyclic imide N (−CON*H-CO−, type 2) sites should equal half of the number of carbonyl C (−C*ONHC*O−, type 4) sites in the monocyclic imide functional group.

(ii) Concentration of imine N (−C═N*−, type 3) sites should equal the number of carbonyl C (−C*═O, type 7) and imine C (C*═N, type 6) sites in the bicyclic imide functional group.

(iii) The number of carbonyl group oxygen (-C═O*) sites should be equal to the number of carbonyl group carbon sites (-C*═O, types 2, 4, and 7).

Therefore, from the N1s spectra the concentrations of the mono- and bicyclic imide functional groups in the material were obtained in a straightforward manner. The concentration of pure polymer was found by subtracting the contribution due to the bicyclic imide functionality from the "combined" peak in the N1s spectra. From the C1s spectra, the concentration of monocyclic imide was obtained by equating the number of monocyclic imide N sites to half the number of monocyclic imide carbonyl carbon sites. The concentration of bicyclic imide functional groups was obtained by evaluating the number of carbonyl/imine carbon sites from the bicyclic imide carbon peak area. The pure polymer concentration was obtained on subtraction of monocyclic imide carbonyl carbon and bicyclic imide carbonyl/imine carbon concentrations from the total carbonyl carbon concentration obtained from the "combined + monocyclic" peak. From the O1s spectra the number of carbonyl group oxygen (−C═O*) sites in the material was evaluated. Excellent agreement was found among the concentration values of the degradation products obtained from C, N, and O core level spectra at different stages of the thermal treatment of the polymer films.

The kinetics of the concentrations of the degradation products thus obtained from the analysis of the XPS spectra are shown in Figure 6. It can be observed from the figure that the thermal degradation of the major part of the polymer occurs within the first 30 min of annealing at the onset temperature of 220 °C. The rate of degradation is observed

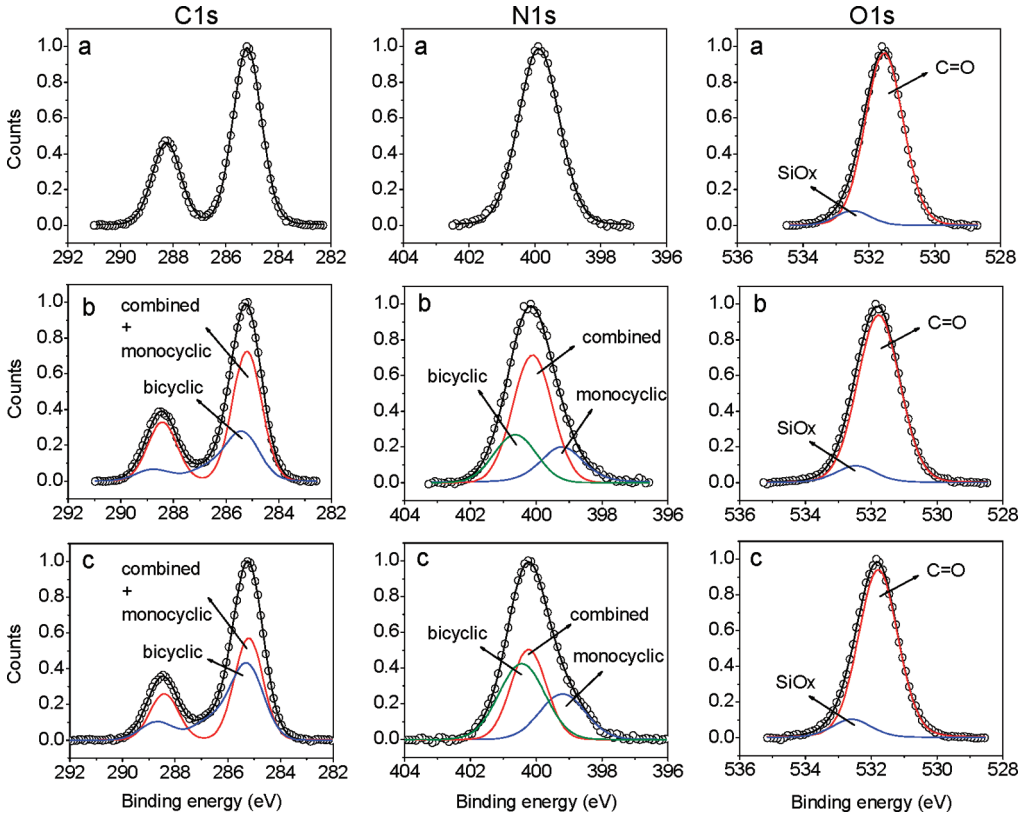

Figure 5. Example curve fits of normalized C, N and O 1s XPS spectra for (a) as-coated sample; sample annealed at the degradation onset temperature 220 °C for (b) 30 min and (c) 8 h. For the definition of the "combined", "monocyclic", and "bicyclic" peaks shown in the C1s and N1s spectra, see the text.

to decrease with duration of thermal treatment and the concentrations of the degradation products almost saturate after about 3 h of annealing. The above results are in excellent agreement with the observations from Figure 4 where it can be found that the major loss of nitrogen and oxygen also takes place within the first 30 min and the saturation time for both cases was between 2 and 4 h. The final degradation product was found to contain about 60% of monocyclic and 40% of bicyclic imide functionalities.

X-ray Reflectivity (XRR). X-ray reflectivity technique was used to study the morphology of thin polymer films. The film was dried at 105 °C under vacuum for about one hour before the study. XRR data was collected *in situ* at 105 °C to study the structure of the thin dry film. The temperature was then increased to 220 °C at a heating rate of 5 °C/min and the sample was annealed for 8 h. XRR studies were conducted at that temperature under vacuum conditions. To obtain information about the thickness, electron density and roughness of the films, the XRR data were analyzed using the Parratt formalism[38] modified to include interfacial roughness.[39] It was observed that the thickness of the film decreases and electron density increases after annealing at 220 °C. We have plotted the data and the fitted reflectivity profiles for the film treated at 105 and 220 °C in Figure 7. The inset of the figure shows the corresponding electron density profiles. The average value of the electron density was obtained by integrating the electron density profile and dividing by corresponding film thickness. From the amplitude of the reflectivity data and the low values of roughness of the annealed film it was clear that the quality of the polymer film remains intact after annealing at the degradation onset temperature for a long time. This indicates

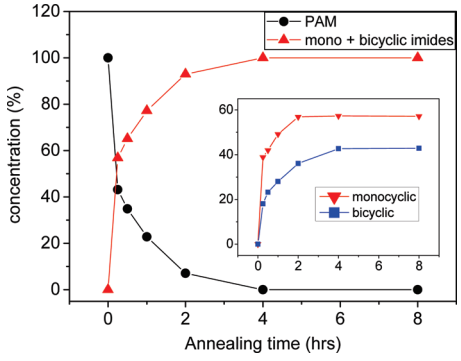

Figure 6. Dynamics of the concentrations of the pure polymer along with that of the major degradation products (monocyclic and bicyclic imide compounds) as obtained from the XPS studies. The inset shows the individual variations of the monocyclic and bicyclic imide compound concentrations with annealing time.

that the interfacial morphology of the film is almost unmodified and the film retains the polymeric property even after undergoing thermal degradation. The structural parameters obtained from fitting of the reflectivity data are shown in Table 2.

4. Conclusions

In conclusion, we have studied thermal degradation of ultrathin polyacrylamide films using NEXAFS, XPS and XRR techniques at the degradation onset temperature (220 °C) of the polymer. NEXAFS and XPS were used for the chemical characterization and XRR was used to study the structure of the degraded films. The chemical analysis of the material revealed that formation of mono- and bicyclic imide functionalities occurs

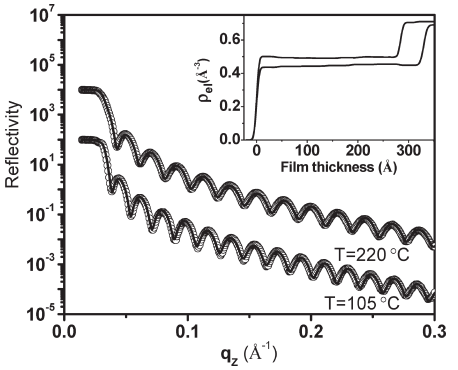

Figure 7. X-ray reflectivity data (symbols) with fitted profiles (solid lines) of the film annealed at 105 and 220 °C. Inset shows corresponding electron density profiles.

Table 2. Various Parameters Obtained from Fits to the Reflectivity Profiles of the Polyacrylamide Film Annealed at 105 and 220 °C

annealing temperature (°C)	film thickness (Å)	top surface roughness (Å)	bottom surface roughness (Å)	average electron density (Å^{-3})
105	330	4.30	5.50	0.45
220	284	3.87	4.38	0.49

on the polymer chains with simultaneous breakdown of amide groups. The kinetics of the degradation products obtained from quantitative analysis of the XPS spectra shows that the thermal degradation of the major part of the polymer occurs within 30 min of annealing at the degradation onset. The rate of degradation is observed to decrease with duration of thermal treatment and the concentrations of the degradation products almost saturate after ~3 h of annealing. The final product was found to contain about 60% of monocyclic and 40% of bicyclic imide functionalities. The structural aspects of the annealed films were studied using X-ray reflectivity (XRR). Analysis of the reflectivity data shows that the thickness of the film decreases and electron density of the film increases after annealing at 220 °C. From the amplitude of the reflectivity data, it was found that the interfacial morphology of the film stays almost unmodified and the film retains the polymeric property even after undergoing thermal degradation.

References and Notes

(1) Bower, D. I. *An introduction to polymer physics*; Cambridge Univ. Press: Cambridge, U.K., 2002.
(2) Flipsen, T. A. C.; Pennings, A. J.; Hadziioannou, G. *J. Appl. Polym. Sci.* **1998**, *67*, 2223–2230.
(3) Ghosh, M. M., Mittal, K. L., Eds.; *Polyimide: fundamental and applications*; Marcel Dekker: New York, 1996.
(4) Harris, F. W. In *Polyimides*; Wilson, D., Stenzenberger, H. D., Hergenrother, P. M., Eds.; Chapman and Hall: New York, 1990.
(5) Marciniec, B. *Hydrosilylation: A Comprehensive Review on Recent Advances*; Springer: Berlin, 2009.
(6) Wang, C.; Stewart, R. J.; Kopecek, J. *Nature* **1999**, *397*, 417–420.
(7) Kopecek, J.; Kopeckova, P.; Minko, T.; Lu, Z. R.; Peterson, C. M. *J. Controlled Release* **2001**, *74*, 147–158.
(8) Singh, A.; Mukherjee, M. *Macromolecules* **2003**, *36*, 8728–8731.
(9) Singh, A.; Mukherjee, M. *Phys. Rev. E* **2004**, *70* (051608), 1–6.
(10) Singh, A.; Mukherjee, M. *Macromolecules* **2005**, *38*, 8795–8802.
(11) Mukherjee, M.; Singh, A.; Daillant, J.; Menelle, A.; Cousin, F. *Macromolecules* **2007**, *40*, 1073–1080.
(12) Mukherjee, M.; Singh, A. *Phys. Stat. Sol. B* **2007**, *244*, 928–942.
(13) Mondal, M. H.; Mukherjee, M. *Macromolecules* **2008**, *41*, 8753–8758.
(14) Mondal, M. H.; Mukherjee, M.; Kawashima, K.; Nishida, K.; Kanaya, T. *Macromolecules* **2009**, *42*, 732–736.
(15) Neto, C. G. T.; Pereira, M. R.; Fonseca, J. L. C. *Polym. Degrad. Stab.* **2002**, *76*, 227–232.
(16) Borman, C. D.; Jackson, A. T.; Bunn, A.; Cutter, A. L.; Irvine, D. J. *Polymer* **2000**, *41*, 6015–6020.
(17) Larlus, O.; Mintova, S.; Valtchev, V.; Jean, B.; Metzger, T. H.; Bein, T. *Appl. Surf. Sci.* **2004**, *226*, 155–160.
(18) Caulfield, M. J.; Qiao, G. G.; Solomon, D. H. *Chem. Rev.* **2002**, *102*, 3067–3084.
(19) Van Dyke, J. D.; Kasperski, K. L. *J. Polym. Sci., Part A: Polym. Chem.* **1993**, *31*, 1807–1823.
(20) Vijayalakshmi, S. P.; Madras, G. *J. Appl. Polym. Sci.* **2006**, *101*, 233–240.
(21) Aarthi, T.; Shaama, M. S.; Madras, G. *Ind. Eng. Chem. Res.* **2007**, *46*, 6204–6210.
(22) de Sainte Claire, P. *Macromolecules* **2009**, *42*, 3469–3482.
(23) Stöhr, J. *NEXAFS Spectroscopy; Springer Series in Sciences*; Springer: Heidelberg, Germany, 1992; Vol. *25*.
(24) Pasquali, L.; De Luisa, A.; Nannarone, S. *AIP Conf. Proc.* **2004**, *705*, 1142–1145.
(25) (a) Nannarone, S.; Borgatti, F.; DeLuisa, A.; Doyle, B. P.; Gazzadi, G. C.; Giglia, A.; Finetti, P.; Mahne, N.; Pasquali, L.; Pedio, M.; Selvaggi, G.; Naletto, G.; Pelizzo, M. G.; Tondello, G. *AIP Conf. Proc.* **2004**, *705*, 450–453.(b) Nannarone, S.; Giglia, A.; Mahne, N.; De Luisa, A.; Doyle, B. P.; Borgatti, F.; Pedio, M.; Pasquali, L.; Naletto, G.; Pelizzo, M. G.; Tondello, G. *Not. Neutroni Luce Sincrotrone* **2007**, *12* (1), 8−19. (http://www.fisica.uniroma2.it/~notiziario/2007/volume12n1.html) [online].
(26) Henke, B. L.; Gullikson, E. M.; Davis, J. C. *At. Data Nucl. Data Tab.* **1993**, *54*, 181–342.
(27) WebCrossSections (http://ulisse.elettra.trieste.it/services/elements/WebElements.html) [online].
(28) Boese, J.; Osanna, A.; Jacobsen, C.; Kirz, J. *J. Electron Spectrosc. Relat. Phenom.* **1997**, *85*, 9–15.
(29) Bullett, N. A.; Talib, R. A.; Short, R. D.; McArthur, S. L.; Shard, A. G. *Surf. Interface Anal.* **2006**, *38*, 1109–1116.
(30) Shard, A. G.; Whittle, J. D.; Beck, A. J.; Brookes, P. N.; Bullett, N. A.; Talib, R. A.; Mistry, A.; Barton, D.; McArthur, S. L. *J. Phys. Chem. B* **2004**, *108*, 12472–12480.
(31) Shikin, A. M.; Gorovikov, S. A.; Adamchuk, V. K.; Molodtsov, S. L.; Engelmann, P.; Laubschat, C. *J. Electron Spectrosc. Relat. Phenom.* **1999**, *105*, 85–90.
(32) Wilks, R. G.; MacNaughton, J. B.; Kraatz, H. -B.; Regier, T.; Moewes, A. *J. Phys. Chem. B* **2006**, *110*, 5955–5965.
(33) Zubavichus, Y.; Zharnikov, M.; Schaporenko, A.; Grunze, M. *J. Electron Spectrosc. Relat. Phenom.* **2004**, *134*, 25–33.
(34) Kikuma, J.; Tonner, B. P. *J. Electron Spectrosc. Relat. Phenom.* **1996**, *82*, 53–60.
(35) Dhez, O.; Ade, H.; Urquhart, S. G. *J. Electron Spectrosc. Relat. Phenom.* **2003**, *128*, 85–96.
(36) Jordan-Sweet, J. L.; Kovac, C. A.; Goldberg, M. J.; Morar, J. F. *J. Chem. Phys.* **1988**, *89*, 2482–2489.
(37) Beamson, G.; Briggs, D., Eds.; *The XPS of Polymers Database*; Surface Spectra Ltd.: Manchester, U.K., 2000.
(38) Parratt, L. G. *Phys. Rev.* **1954**, *95*, 359–369.
(39) Russell, T. P. *Materials Science Reports*; Elsevier North-Holland: Amsterdam, 1990; Vol. *5*.